PHYSICAL REVIEW E **85**, 061705 (2012)

Surface and bulk contributions to nematic order reconstruction

A. Amoddeo,[1,*] R. Barberi,[2,3,†] and G. Lombardo[3,*]

[1]*Mechanics and Materials Department, Università "Mediterranea" di Reggio Calabria, I-89122 Reggio Calabria, Italy*
[2]*Physics Department, Università della Calabria, I-87036 Rende (CS), Italy*
[3]*CNR-IPCF UOS di Cosenza, c/o Università della Calabria, I-87036 Rende (CS), Italy*

(Received 20 December 2011; published 18 June 2012)

Nematic molecules confined in an asymmetric π cell and subjected to strong electric fields exhibit textural distortions involving nematic order variations, described by the Landau-de Gennes **Q**-tensor theory. We investigated the evolution of order variations as function of the applied electric pulse amplitude and of the nematic surface pretilt anchoring angles by implementing a **Q**-tensor model with a moving mesh finite element method. The proposed technique is able to clearly distinguish the bulk and the surface order reconstruction which occur in the cell.

DOI: 10.1103/PhysRevE.85.061705 PACS number(s): 64.70.mf, 61.30.Gd, 61.30.Hn, 61.30.Dk

I. INTRODUCTION

Isotropic liquids are ergodic systems for which a time average is equivalent to a space average, entailing a random molecular orientation [1]. Conversely, molecules in a solid crystalline phase are forced by the intermolecular interactions to lie, on average, in a lattice structure. Thermotropic liquid crystals (LCs) in the nematic phase, instead, consist of calamitic (i.e., rod-shaped) molecules, which, in a temperature range between the isotropic liquid and the crystalline state, exhibit long-range orientational order. Classically, the nematic phase is described by the Frank-Oseen theory [2], where, usually, the director **n**, pointing out the average molecular orientation, varies in space, and the degree of orientational order, described by the scalar order parameter S, is considered practically constant everywhere. This theory is able to describe elastic monostable transitions, as in the case of Freedericks phenomena, where the starting nematic texture, prescribed by suitable boundary conditions, is elastically distorted by an external electric or magnetic field, and the induced distortion always relaxes back to its initial equilibrium texture when the external perturbation is removed.

Some physical phenomena occurring in highly frustrated LC systems deserve particular interest and cannot be fully explained by this simplified classical description, such as LC confined by means of topographic patterns [3], LC emulsions [4], LC confined in porous materials [5], topological defects [6–8], or self-organized colloidal dispersions in LC [9–11]. In fact, in all these cases, the nematic distortion occurs over a length scale comparable with the biaxial coherence length ξ_b [12], the nematic order varies, and biaxial domains arise inside the nematic phase, resulting in the relaxation of the strong distortion. Consequently, the more sophisticated theory based on the Landau de Gennes order tensor **Q** [13] needs to be defined in order to obtain reliable results: In this frame, domains having uniaxial order present a cylindrical symmetry with respect to the director and a unique optical axis, while in biaxial ordered domains such symmetry is broken and the system presents two distinct optical axes. However, most nematogenic molecules are intrinsically biaxial, even if they give rise to a uniaxial phase, which usually is a consequence of the rotational disorder around the long molecular axis. If the rotational disorder is hampered, non-uniaxial features may appear and biaxial order could arise [14].

Biaxial domains can grow within uniaxial LC systems in the bulk as well at the LC interface [15–18], and, recently, much effort has gone into understating their theoretical foundation. Recent experiments on LC frustrated systems show that local and transient bulk biaxial order can be induced inside a nematic phase, suggesting that biaxiality plays a fundamental role in LC phenomena which take place on a nanometric scale [19–24]. In particular, the biaxial order reconstruction in nematics has been proposed as a new tool capable of connecting two competing uniaxial nematic textures by means of transient biaxial states [19]. In fact, applying a strong electric field inside a symmetric π cell, it is possible to transform the initial splay texture into the topological different bend one by changing the local order of the nematic phase without any macroscopic director rotation. Moreover, it has been experimentally and theoretically demonstrated that, by nanoconfining a nematic topological defect, the nematic phase undergoes a structural transition with predominant biaxial order [24]. Such phenomena are mathematically described by the order tensor **Q,** where the eigenvectors point out the preferred molecular orientation while the associated eigenvalues measure the degree of order [25,26].

Very recently, electrically induced nematic order reconstruction has been investigated experimentally as well as theoretically within an asymmetric π cell with strong anchoring energy [27,28]. As the starting splay texture is not symmetric with respect to the midplane of the cell, the electrically induced biaxial wall occurs near a confining surface layer and the π-bend texture grows at the expense of the starting splay texture, overcoming the topological barrier. With the electro-optical as well as the electric threshold observations comparable with the corresponding of the surface anchoring breaking phenomenon [29], the mechanism governing the real process allowing us to overcome the topological barrier between the splay-bend textures needs further studies, and a more sophisticated numerical technique is required in order to thoroughly investigate what happens when the induced

---

[*] Corresponding authors: antonino.amoddeo@unirc.it, giuseppe.lombardo@cnr.it

[†] riccardo.barberi@fis.unical.it

distortion occurs close to a confining surface of a π cell, as new effects could arise [30].

In this work, we use the finite element method (FEM) in order to solve the time-dependent $\mathbf{Q}$ tensor governing equations inside an asymmetric π cell submitted to high electric fields, implementing a moving mesh partial differential equations (MMPDE) numerical technique. The MMPDE technique, belonging to the class of r-type adaptive grid techniques, ensures no waste of computational effort in areas where there is no need for finer grids: The nodal connectivity and the number of mesh points inside the domain are kept constant while the mesh points themselves are moved into regions where more detail is required [31]. This peculiarity is fundamental for our investigated system; in fact, since the spatial position at which the biaxial domains can occur is *a priori* unknown, the adaptive method proposed is capable of moving the nodes toward regions where the gradient of $\mathbf{Q}$ is growing, allowing, thus, a greater resolution [32,33]. Moreover, for a given spatial resolution, since the number of nodes is kept fixed, a smaller number of mesh points are needed with respect to simulations performed on uniform grids, resulting in a saving of computational costs.

The paper has the following structure: In Sec. II we provide the basic details of the $\mathbf{Q}$ tensor model used to describe the dynamical behavior of a nematic phase, as theoretical details have been thoroughly addressed in Refs. [26,32,33]; in Sec. III we introduce the used computational technique and the physical parameters used for the simulation. In Sec. IV we present and discuss our numerical results, and, finally, we conclude in Sec. V.

II. BASIC THEORY

The order of a nematic liquid crystal texture can be described by the order tensor

$$\mathbf{Q} = \sum_{i=1}^{3} s_i \boldsymbol{u}_i \otimes \boldsymbol{u}_i, \tag{1}$$

where each $\boldsymbol{u}_i$ is an orthogonal unit vector representing an eigenvector of $\mathbf{Q}$ and s_i are the corresponding eigenvalues. In the isotropic phase, the calamitic molecules do not present any orientational order; all the eigenvalues vanish and the optical behavior is like an isotropic fluid. The uniaxial nematic phase is described by the eigenvector associated to the maximum eigenvalue $s_{\max}$, giving the scalar order parameter $S = (3/2)s_{\max}$, while the remaining two eigenvalues are equal, and a unique optical axis is present. In the biaxial nematic phase, all three eigenvalues differ. From Eq. (1) it follows that $\mathbf{Q}$ is symmetric, and it is also imposed to be traceless [13,25]. In order to describe nematics in biaxial configurations, a complete representation of Eq. (1) is required, and $\mathbf{Q}$ is a tensor field as the order changes locally from point to point.

The degree of biaxiality is measured using the definition [19]

$$\beta^2 = 1 - 6\frac{\mathrm{tr}(\mathbf{Q}^3)^2}{\mathrm{tr}(\mathbf{Q}^2)^3} \in [0,1]. \tag{2}$$

When $\beta^2 = 0$, the nematic texture is uniaxial; instead, the maximum of biaxiality corresponds to $\beta^2 = 1$, when the nematic phase is biaxial. The condition of $\mathbf{Q} = \mathbf{0}$ corresponds to a local order loss, and, in this case, nematics are in an isotropic phase.

To model the $\mathbf{Q}$-tensor response of a nematic to an external field, the minimization of the free energy density functional $\mathcal{F}$ inside the cell containing the liquid crystal is required. Contributions to $\mathcal{F}$ are assumed to originate from bulk only, since surface terms are neglected because of the fixed boundary conditions imposed, thus leading to infinite anchoring strength. Consequently,

$$\mathcal{F} = \int_V (F_d + F_t + F_e)\,dV, \tag{3}$$

where the integration is performed over the domain volume V and the thermotropic, electric, and elastic terms, respectively, F_t, F_e, and F_d, are expressed in powers of $\mathbf{Q}$, assuming their dependence from small $\mathbf{Q}$ distortions. Hence,

$$F_t = F_t(\mathbf{Q}), \quad F_e = F_e(\mathbf{Q},\nabla\mathbf{Q}), \quad F_d = F_d(\mathbf{Q},\nabla\mathbf{Q}), \tag{4}$$

where

$$F_t = a\,\mathrm{tr}(\mathbf{Q}^2) - \frac{2b}{3}\mathrm{tr}(\mathbf{Q}^3) + \frac{c}{2}\left(\mathrm{tr}(\mathbf{Q}^2)\right)^2, \tag{5}$$

with $a = \alpha(T - T^*) = \alpha\Delta T$, $\alpha > 0$, where T^* is the supercooling temperature [13] and b and c are approximated as constants and

$$F_e = -\frac{\varepsilon_0}{2}\left(\varepsilon_i\left|\nabla U\right|^2 + \varepsilon_a \nabla U \cdot \mathbf{Q}\nabla U\right) + \bar{e}\nabla\mathbf{Q}\cdot\nabla U, \tag{6}$$

where ε_0 is the vacuum electric permeability and ε_i and ε_a are the isotropic and the anisotropic dielectric susceptibilities defined as

$$\varepsilon_i = \frac{(\varepsilon_\parallel + 2\varepsilon_\perp)}{3}, \quad \varepsilon_a = \frac{(\varepsilon_\parallel - \varepsilon_\perp)}{S_{\mathrm{eq}}}, \tag{7}$$

with $\varepsilon_\parallel$ and $\varepsilon_\perp$ dielectric nematic constants respectively parallel and perpendicular to the molecular axis and where U is the electric potential. In Eq. (6) the last term accounts for polarization effects in which

$$\bar{e} = \frac{e_{11} + e_{33}}{2S_{\mathrm{eq}}} \tag{8}$$

while e_{11} and e_{33} are the splay and bend flexoelectric coefficients, respectively. In Eqs. (7) and (8)

$$S_{\mathrm{eq}}(\Delta T) = \frac{b}{4c}\left(1 + \sqrt{1 - \frac{24ac}{b^2}}\right) \tag{9}$$

is the equilibrium order parameter for uniaxial systems. Finally, the elastic contribution to the free energy functional is given by

$$F_d = \frac{L_1}{2}\left(\frac{\partial Q_{ij}}{\partial x_k}\right)^2 + \frac{L_2}{2}\frac{\partial Q_{ij}}{\partial x_j}\frac{\partial Q_{ik}}{\partial x_k} + \frac{L_6}{2}Q_{lk}\frac{\partial Q_{ij}}{\partial x_l}\frac{\partial Q_{ij}}{\partial x_k} \tag{10}$$

with

$$\begin{aligned} L_1 &= \frac{1}{6S_{\mathrm{eq}}^2}(k_{33} - k_{11} + 3k_{22}) \\ L_2 &= \frac{1}{S_{\mathrm{eq}}^2}(k_{11} - k_{22}) \\ L_6 &= \frac{1}{2S_{\mathrm{eq}}^3}(k_{33} - k_{11}) \end{aligned} \tag{11}$$

and where k_{11}, k_{22}, and k_{33} are the Frank elastic constants.

The order tensor can be written in terms of five independent parameters q_i, $i \in [1,5]$, corresponding to the degrees of freedom of a rodlike nematic molecule

$$\boldsymbol{Q} = \begin{pmatrix} q_1 & q_2 & q_3 \\ q_2 & q_4 & q_5 \\ q_3 & q_5 & -q_1 - q_4 \end{pmatrix}. \tag{12}$$

The evolution equations are represented by the generalized Euler-Lagrange equation giving the partial differential equations (PDE) system

$$\frac{\partial D}{\partial \dot{q}_i} + \frac{\partial F_t}{\partial q_i} + \frac{\partial F_e}{\partial q_i} + \frac{\partial F_d}{\partial q_i} - \frac{\partial}{\partial x_j}\left(\frac{\partial F_d}{\partial q_{i,j}}\right) - \frac{\partial}{\partial x_j}\left(\frac{\partial F_e}{\partial q_{i,j}}\right) = 0 \quad i = 1\ldots5, \tag{13}$$

which is solved imposing Dirichlet boundary conditions on the boundary surfaces, together with the governing equation for the electric potential

$$\nabla \cdot \boldsymbol{D} = \nabla \cdot (-\varepsilon_0 \boldsymbol{\varepsilon} \nabla U + \boldsymbol{P}_S) = 0. \tag{14}$$

In Eq. (14), $\boldsymbol{D}$ is the displacement field, $\boldsymbol{\varepsilon}$ is the dielectric tensor, and $\boldsymbol{P}_s$ is the spontaneous polarization vector [37,38] required to fulfill the Maxwell equations in absence of free charges.

The system (13), in which summation over repeated indices is assumed and where the subscript "j" denotes differentiation with respect to the spatial coordinates x_1, x_2, and x_3, is attained starting from the balance equation [34,35]

$$\delta D + \delta \dot{F} = 0, \tag{15}$$

where D is the Rayleigh dissipation function given as

$$D = \int_V D dV = \int_V \gamma \mathrm{tr} \dot{\mathbf{Q}}^2 dV, \tag{16}$$

with D dissipation function density and γ related to the rotational viscosity; further, the backflow is neglected [36], and the variation of the dissipation function density is expressed as

$$\frac{\partial D}{\partial \dot{q}_i} \delta \dot{q}_i = 2\gamma \mathrm{tr}\left(\dot{\mathbf{Q}} \frac{\partial \mathbf{Q}}{\partial q_i}\right) \delta \dot{q}_i. \tag{17}$$

III. COMPUTATIONAL METHOD AND SETTINGS

In order to solve the PDE system arising from Eqs. (13) and (14) by FEM, implementing the MMPDE numerical technique [32,33], the appropriate discretization of the integration domain is obtained by applying the *equidistribution principle* [39,40]. This method allows us to control the mesh map quality by means of a monitor function [41–43] where the optimal choice depends on the problem being solved, the numerical discretization being used, and the norm of the error that is to be minimized [42], allowing accurate representations of sharp solution features, such as shocks or defects.

For a one-dimensional problem (1D), let z be the physical coordinate, specifically, our cell thickness, and $u(z,t)$ a solution over a physical domain $\Omega_p = [0,1]$ of a PDE system, we then introduce a fixed computational domain $\Omega_c = [0,1]$ with ξ computational coordinate. It follows that a one-to-one mapping at time t from computational to physical space is defined by the coordinate transformation from computational space $\Omega_c \times (0,T]$ to physical space $\Omega_p \times (0,T]$,

$$z = z(\xi,t), \quad \xi \in \Omega_c, \quad t \in (0,\mathrm{T}], \tag{18}$$

while the inverse from physical space $\Omega_p \times (0,T]$ to computational space $\Omega_c \times (0,T]$ is represented as

$$\xi = \xi(z,t), \quad z \in \Omega_p, \quad t \in (0,\mathrm{T}]. \tag{19}$$

Imposing a uniform grid on computational space,

$$\xi_i = i/N, \quad i = 0,1,\ldots,N \tag{20}$$

gives a set of nodes on physical space

$$0 = z_0(t) < z_1(t) < \ldots z_N(t) = 1 \tag{21}$$

corresponding to an equispaced grid in the computational space. The mesh map quality control is attained by equidistributing a monitor function $M(u(z,t))$ over the integration domain [39,41–44]:

$$\int_0^{z(\xi,t)} M(u(s,t))ds = \xi \int_0^1 M(u(s,t))ds. \tag{22}$$

Differentiating the integral form of the equidistribution principle, Eq. (22), its differential form is obtained,

$$\mathrm{M}(z(\xi,t)) \frac{\partial}{\partial \xi} z(\xi,t) = \int_0^1 M(u(s,t))ds = C(t), \tag{23}$$

representing the mesh equation giving the node coordinates $z(\xi,t)$ on which the problem is solved. The latter expression clearly shows that, in order to keep the distribution of the monitor function constant over the integration domain, a larger monitor function value must correspond to a denser mesh.

The choice of the monitor function was addressed to that tested by Beckett *et al.* [39], belonging to a method proposed by Huang *et al.* [44], since it ensures a good quality control of the meshes and final convergence of the FEM solution [39,41,42],

$$\mathrm{M}(u(z,t)) = \int_0^1 \sqrt{\left|\frac{\partial u(z,t)}{\partial z}\right|} dz + \sqrt{\left|\frac{\partial u(z,t)}{\partial z}\right|}. \tag{24}$$

The advantages derived from using this function, as well the numerical procedure and the algorithm description, have been thoroughly examined in Refs. [32,33]. Summarizing, we have a multidimensional time-dependent problem, and the overall adaptive solution process involves the modelling of the physical problem with a 1D π cell with infinite anchoring energy on both plates, to which an electric pulse is applied perpendicularly. At time $t = 0$ s, the mesh points are uniformly distributed over the integration domain, and at the current time step the five coupled PDE resulting from the Euler-Lagrange equations (13) and the Maxwell equation for the electric potential inside the cell (14) are solved, obtaining, at each time step, six unknown exact solutions $u(z,t)$. The problem then is tackled with an iterative process involving the following: (a) generation of the adaptive moving mesh evaluating the monitor function for the current time step and (b) solution of Eqs. (13) and (14) for the current mesh and updating the solution for the next time step.

The second step is based on relaxation methods [45], and the computations were carried out using the COMSOL MULTIPHYSICS finite element package with MATLAB [46]. The Galerkin's method associated to a weak formulation of the residuals of the differential equations [47] allowed us to overcome the nonlinearity of the problem. Ritz's method applied to Eq. (14), instead, allowed us to calculate the potential distribution.

It is well accepted [19] that, inside a π cell, two topologically different nematic textures are possible: In the first one, the nematic director is almost parallel to the boundary plates with a slight splay deformation and, in the second one, the nematic is almost perpendicular to the plates and presents a bend deformation which is topologically equivalent to a twisted configuration, i.e., a nematic texture with a π torsion. Due to the surface treatment on the internal boundary plates, the nematic molecules confined between them are aligned on both surfaces with strong anchoring energy with a fixed pretilt angle θ. In addition, letting the pretilt angle be oppositely directed by means of an antiparallel arrangement, an initial splay configuration of the nematic texture establishes inside the cell. The spontaneous relaxation from the splay toward the bend/twisted texture is prevented by the arising energy barrier which depends on the tilt angle and on the ratio of elastic moduli. The switching between the two textures is possible if, breaking the starting nematic texture somewhere, it is allowed to connect the two topologically different textures. Among different suitable switching mechanisms [7,24], the nematic biaxial order reconstruction induced by the electric field [19–23,26] is a possible one enabling the escape from topological constraints and overcoming the energy barrier.

The FEM procedure used involves the solution of Eqs. (13) and (14) at each time step using a quadratic finite element approximation, replacing in Eqs. (24) the exact solution $u(z,t)$ with $\mathrm{tr}(\mathbf{Q}^2)$: such a quantity is suitable to monitor order reconstruction phenomena, since it is the sum of the squared **Q** eigenvalues, which rapidly vary when the degree of order is not constant.

We performed our calculations simulating a cell 1 μm thick, with asymmetric anchoring conditions of nematic molecules on the boundary plates, setting the anchoring angles, both measured with respect to the plates, on the lower boundary surface to $\theta_l = 19^\circ$ and on the upper boundary surface to $\theta_u = 0^\circ, -1^\circ, -2^\circ, -3^\circ$. The electric pulse is applied at $t = 0$ s, for a duration of 0.25 ms, along the z direction, with amplitudes from 10 to 14 V/μm. The physical parameters, used to sample the dynamical evolution of the **Q** tensor with a time step size of $\Delta t = 0.1$ μs, are those already used for a 5CB nematic liquid crystal [26,32,33], with $\Delta T = -1\,^\circ$C [48]. For a symmetric π cell having $\theta_l = 19$ and $\theta_u = -19^\circ$ we find an electric order reconstruction threshold $E_{\mathrm{th}} = 8$ V/μm, in agreement with previous reported theoretical and experimental values [19,22]. On the other hand, it has been seen that asymmetric anchoring conditions imposed on a π cell containing a 5CB nematic LC cause variations in E_{th} [28], which need more investigations. We have monitored the biaxiality arising along the cell thickness, Eq. (2), at the various electric field amplitudes, discretizing the physical domain with a mesh of 285 grid points. In addition, assuming nematic molecules as a purely dielectric material and neglecting ion effects, for each amplitude of the applied field we have evaluated also the density of the current flowing across the cell, a quantity which is very sensitive to changes of the nematic order [20,28], using the expressions derived in Ref. [19],

$$J = \frac{U}{d}\frac{d}{dt}\left(\frac{1}{\overline{\varepsilon_{\mathrm{eff}}^{-1}}}\right), \qquad (25)$$

and setting $\Delta\varepsilon = \varepsilon_{\parallel} - \varepsilon_{\perp}$

$$\varepsilon_{\mathrm{eff}} = \varepsilon_0\left(\sqrt{\frac{2}{3}}\Delta\varepsilon\, \mathrm{Q}_{zz} + \varepsilon_i\right), \quad \overline{\varepsilon_{\mathrm{eff}}^{-1}} = \frac{1}{d}\int_{-\frac{d}{2}}^{\frac{d}{2}} \frac{1}{\varepsilon_{\mathrm{eff}}} dz. \qquad (26)$$

Equations (26) are a consequence of the one-dimensional nature of our problem, in which all fields depend only on the z coordinate.

IV. NUMERICAL RESULTS AND DISCUSSION

Nematic LCs confined in a π cell with strong and asymmetric anchoring conditions, similarly to the symmetric case [19,21,32,33,49], can present two topologically different textures, splay and π bend/twist. The imposed asymmetry as well the strong anchoring conditions allow us to concentrate the largest nematic distortion close to the surface where the nematic molecules have anchoring angles approaching planar conditions, in our case close to the upper cell surface [28]. The evolution of the electrically induced distortion is monitored calculating the local biaxiality arising in a region close to the upper boundary plate, for different upper pretilt angles and imposing electric pulses with increasing amplitude. Each Figs. 1 to 5 shows the induced biaxiality during the application of electric pulses of amplitudes 10, 11, 12, 13, and 14 V/μm. Moreover, when going from panel (a) to panel (d), the upper anchoring angle varies from $\theta_u = -3$ to $\theta_u = 0^\circ$ with step $\Delta\theta = 1^\circ$. The vertical and the horizontal axes correspond, respectively, to the cell thickness in the 0.9 μm $\leqslant z \leqslant 1$ μm range and to the time scale of the solution evolution in the 0 ms $\leqslant t \leqslant 0.1$ ms interval. The biaxiality is linearly mapped in a grey levels scale between the black (zero biaxiality) and white (maximum biaxiality) colours.

In Fig. 1(a), a $t = 0$ s, the initial nematic texture is in an asymmetric splayed configuration and the nematic molecules next to the upper surface stay almost planar to the plate. After the application of the electric field of amplitude 10 V/μm, for $t > 0$ s, the molecules start to align their director along the field direction, and a biaxial region of thickness comparable with the biaxial coherence length ξ_b starts to grow, connecting the surface planar nematic texture with the competing vertical bulk nematic molecules [19,32,33]. The strong induced nematic distortion relaxes by lowering the nematic order, i.e., the starting uniaxial phase is lost and it is locally replaced by growing biaxial domains. At $t = 48$ μs the induced biaxial region looks like a crater of a volcano, where the biaxiality is zero inside and around the crater [4,19]: This is the signature of the order reconstruction phenomenon; for $t > 50$ μs the biaxial wall disappears, meaning that the initial splayed texture is replaced by a bend. The uniaxial order is restored everywhere except for a residual biaxiality near the upper surface due to the strong anchoring energy.

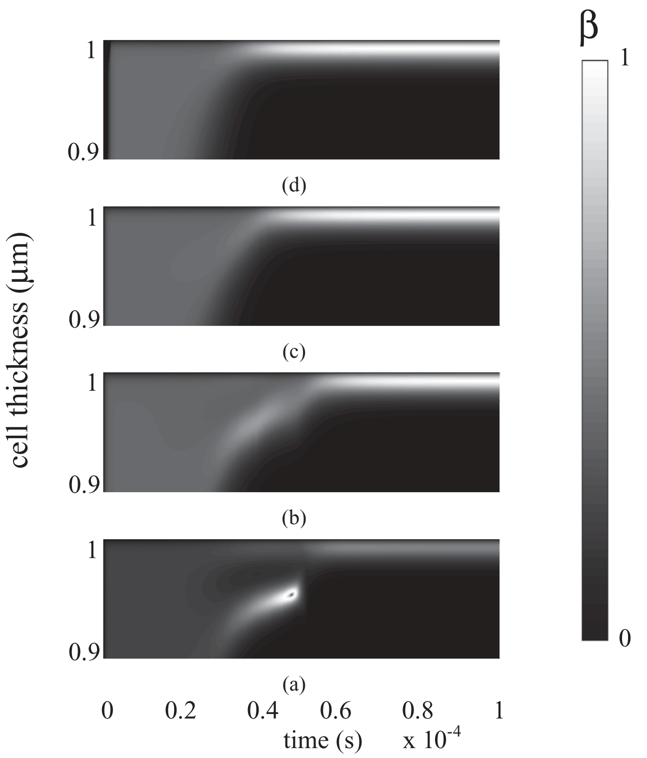

FIG. 1. Surface contour plots of the biaxial order evolution, close to the upper boundary plate, for an electric pulse of amplitude 10 V/μm. The vertical and the horizontal axes correspond to the cell thickness in the 0.9 μm $\leqslant z \leqslant$ 1 μm range and the time scale of the solution evolution in the 0 ms $\leqslant t \leqslant$ 0.1 ms interval, respectively: (a) $\theta_u = -3^\circ$, (b) $\theta_u = -2^\circ$, (c) $\theta_u = -1^\circ$, and (d) $\theta_u = 0^\circ$. The biaxiality is linearly mapped in a gray scale between the black (zero biaxiality) and white (maximum biaxiality) colors.

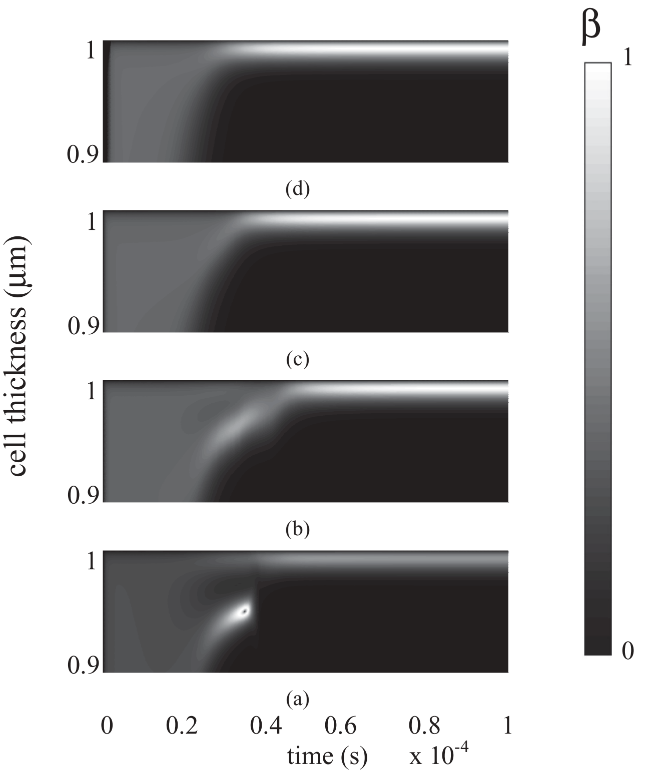

FIG. 2. As in Fig. 1 but with an amplitude for the electric pulse of 11 V/μm.

For $\theta_u = -2^\circ$, Fig. 1(b), the volcano-like biaxial region is not present, but a bulk biaxiality clustered around 38 μs starts to develop and propagate inside the cell. In fact, the electrically induced bulk strain is pushed toward the upper surface, and, at the same time, S becomes strongly inhomogeneous and a thin biaxial film of thickness comparable with the electric coherence length ξ_E grows. For $t > 50$ μs, the induced nematic strain is completely absorbed by the upper surface layer: the distortion energy cost less on that surface layer because the elastic constants, which are proportional to S^2, present lower values of S.

For $\theta_u = -1^\circ$, Fig. 1(c), the biaxial cluster also disappears, and the biaxiality is almost all concentrated close to the upper boundary surface; the same behavior occurs for $\theta_u = 0^\circ$, Fig. 1(d). In general, holding the amplitude of the applied electric field constant and decreasing θ_u from -3° to 0°, the electrically induced nematic distortion relaxes by means of two different mechanisms: a fast one involving the appearance of the order reconstruction phenomenon [19] and a slow one involving the motion of the bulk biaxiality toward the low pretilt surface plate, on which it finally spreads [28]. In fact, for $\theta_u = -3^\circ$, the splay-bend transition presents a complete order reconstruction evolution similar to what happens within a symmetric π cell. Otherwise, at lower θ_u, the induced nematic strain is absorbed on the upper surface, where the growth of the surface biaxial layer mediates the competition between the bulk reorientation due to the high electric field and the

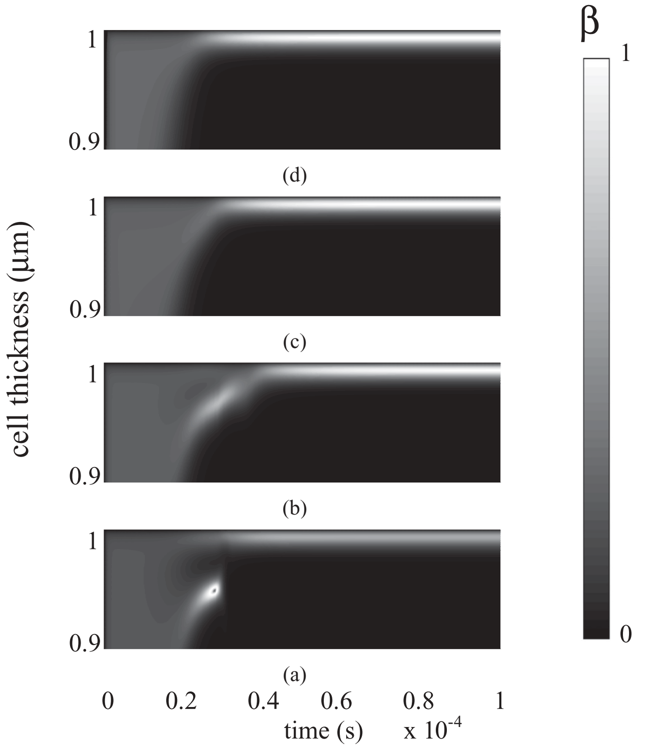

FIG. 3. As in Fig. 1 but with an amplitude for the electric pulse of 12 V/μm.

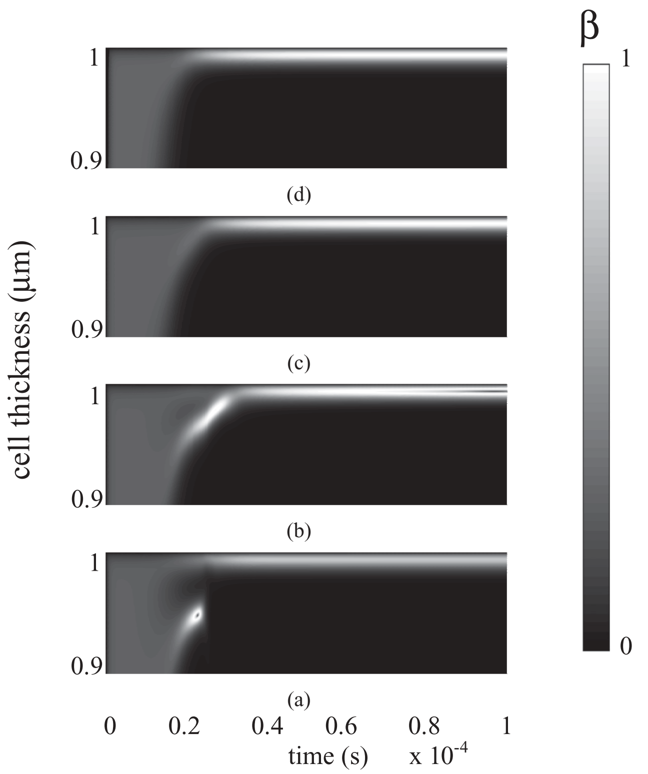

FIG. 4. As in Fig. 1 but with an amplitude for the electric pulse of 13 V/μm.

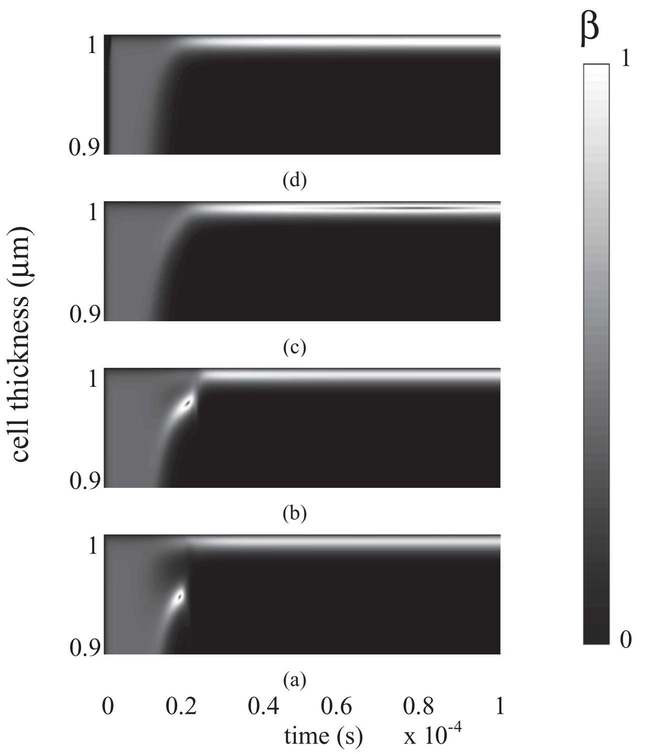

FIG. 5. As in Fig. 1 but with an amplitude for the electric pulse of 14 V/μm.

surface local order which cannot change due to the strong anchoring energy. Applying higher amplitudes of electric field, the same two different textural switching mechanisms occur faster and, moreover, it is possible to achieve the order reconstruction transition closer to the upper surface layer. By the way, Fig. 4(b) shows what happens when the nematic distortion is pushed by an applied electric field amplitude of 13 V/μm toward the upper boundary surface where $\theta_u = -2^\circ$: The nematic phase, under the combined effect of the planar alignment with strong anchoring energy and the vertical alignment enforced by the electric field, loses its natural uniaxial symmetry, showing biaxial features [26,50]. In particular, at $t = 95$ μs, the surface order reconstruction occurs which extends for a few microseconds. The same mechanism occurs at a lower pretilt angle, markedly at $\theta_u = -1^\circ$, increasing the electric field amplitude to 14 V/μm, see Fig. 5(c), and, looking at the evolution of the nematic director in the last 10 μm close to the upper boundary plate, can help to understand the switching mechanism driven by the surface order reconstruction transition. In fact, the magnifications of Fig. 6 shows that, at $t = 20$ μs, Fig. 6(a), the nematic texture is quite distorted, the biaxiality is already relevant, see Fig. 5(c), and, when going toward the bulk, the nematic molecules tend to be aligned along the direction of the electric field. At $t = 75$ μs, Fig. 6(b), the molecules lying close to the upper plate approach a planar uniaxial configuration, while the bulk molecules are in a vertical configuration. At $t = 79$ μs, Fig. 6(c), corresponding to the uniaxial dip inside the surface biaxial wall of Fig. 5(c), the molecules are in a vertical configuration, except for the planar uniaxial state close the upper confining plate. Soon after, at $t = 83$ μs, Fig. 6(d), the nematic configuration is symmetric with respect to Fig. 6(b). For $t > 100$ μs, for instance, at $t = 114$ μs as in Fig. 6(e), the splay-bend transition of the nematic texture is completed. The nematic director configuration inside the whole π cell, instead, is shown in Fig. 7 for $t = 0$ s (a), for $t = 0.25$ ms (b), and after the electric field was switched-off (c), at $t = 0.26$ms. It can be seen that the nematic texture starts from a splay configuration, Fig. 7(a); at the end of the electric pulse is in a vertical state, Fig. 7(b); while for $t > 0.25$ ms, Fig. 7(c), the director suffers a spontaneous viscoelastic relaxation [26], a behavior which is common to all the investigated cases. From our computations, it seems that a lowering of the pretilt angle cause a rise of the electric amplitude threshold required for the bulk order reconstruction transition to take place.

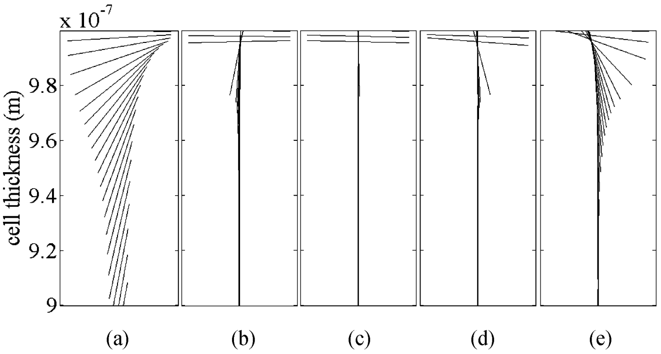

FIG. 6. Nematic director evolution in the last 10 μm close to the upper boundary plate of the π cell subjected to an electric pulse with amplitude 14 V/μm for a duration of 0.25 ms, and for $\theta_u = -2^\circ$, at different times: (a) 20 μs, (b) 75 μs, (c) 79 μs, (d) 83 μs, (e) 114 μs.

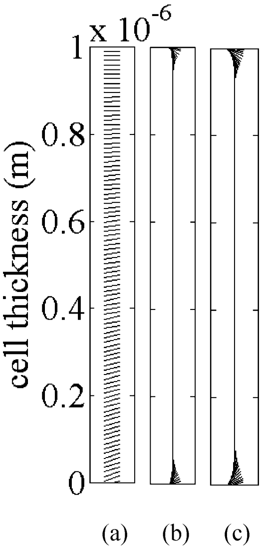

FIG. 7. Nematic director configuration across the π cell subjected to an electric pulse with amplitude 14 V/μm for a duration of 0.25 ms, and for $\theta_u = -2^\circ$, at different times: (a) 0 s, (b) 0.25 ms, (c) 0.26 ms.

We observe that the induced nematic distortion is moved, temporally by the variations of the electric field amplitude and both spatially and temporally by the variations of the upper pretilt angle. It is worth noting as at lower pretilt angles, the order reconstruction is no longer a bulk phenomenon but a surface one.

Figures 1–5, show that, at a given amplitude of the electric pulse, biaxiality arises where the nematic distortion, i.e., $\nabla\mathbf{Q}$, is higher, as a consequence of the strong competition between the vertical alignment due to the electric field and the planar alignment of the surface nematic layer. The proposed numerical technique concentrates the mesh points in regions of high spatial order variability and, at the same time, pulls them away from regions of low distortion, and, consequently, it is possible to capture the relevant biaxial features that occur close to the surface layer [28,32,33].

Very recently, analysis of the current signal coming from an asymmetric π cell allowed us to distinguish the dynamical order behavior giving relevant data about the induced biaxiality and the different relaxation mechanisms [28]. Figures 8–12 show the calculated electric current flowing across the cell during the application of the above electric field amplitudes, where curves (a) to (d) refer to the four different pretilt upper surface angles. In each figure, the first and faster broad structure is related to the dielectric molecular reorientation along the field direction, and whatever the amplitude of the applied electric pulse is, for $\theta_u = 0^\circ$, nothing else other than this peak is present, see Figs. 8(d)–12(d). Applying a pulse with amplitude 10 V/μm and $\theta_u = -3^\circ$, curve 8(a), a distinct peak is evident at 50 μs which is related to the breaking of the biaxial wall, see Fig. 1(a) [19,33]. Decreasing the anchoring angle to $\theta_u = -2^\circ$, curve 8(b), apart from the fastest peak, a smooth and lasting structure is present, partially superimposed on the tail of the dielectric peak, centred around 45 μs and due to the slow movement of the planar wall toward the upper surface layer [28], see also Fig. 1(b). Such a structure is not so evident for $\theta_u = -1^\circ$ since it becomes totally superimposed on the tail of the dielectric peak, Figure 8(c). Increasing the amplitude of the electric field up to 14 V/μm, Figs. 9–12, all the structures, including the first peak, become faster [33]. In addition, with $\theta_u = -2^\circ$ and a pulse amplitude of 13 V/μm, the smooth current structure become less evident, Fig. 11(b), and, increasing the amplitude to 14 V/μm, Fig. 12(b), it is suddenly replaced by a sharper and faster one characterizing the order reconstruction transition, see Fig. 5(b). The current computations in Figs. 11 and 12 reveal slight topological variations not captured by the biaxiality and reflect the biaxial evolution seen in Figs. 4 and 5, except for the surface order reconstruction transition observed in Figs. 4(b) and 5(c): In these cases the nematic distortion becomes progressively confined in a very few nematic layers close to the upper boundary surface where the biaxiality is nearly constant and the uniaxial order is slowly varying over a wide time interval. Given that the current flowing between the plates is proportional to a time derivative of the order tensor $\mathbf{Q}$ [19], it follows that the contribution to the current coming from the upper boundary region is negligible if compared to the contribution coming from the bulk region, and, consequently, no related structure are expected to be visible in the current computations.

If the amplitude of the applied field is kept below 13 V/μm, the biaxiality velocity increases according to decreasing

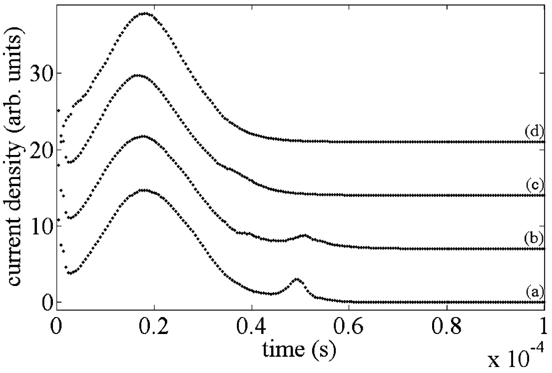

FIG. 8. Computation of the electric current density flowing across the cell in the 0 ms $\leqslant t \leqslant$ 0.1 ms time interval for an electric pulse of amplitude 10 V/μm: (a) $\theta_u = -3^\circ$, (b) $\theta_u = -2^\circ$, (c) $\theta_u = -1^\circ$, and (d) $\theta_u = 0^\circ$.

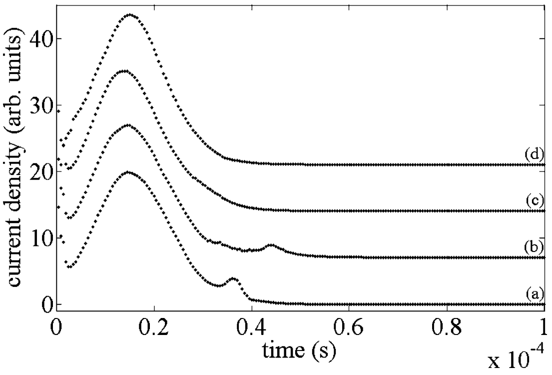

FIG. 9. As in Fig. 6 but with an amplitude for the electric pulse of 11 V/μm.

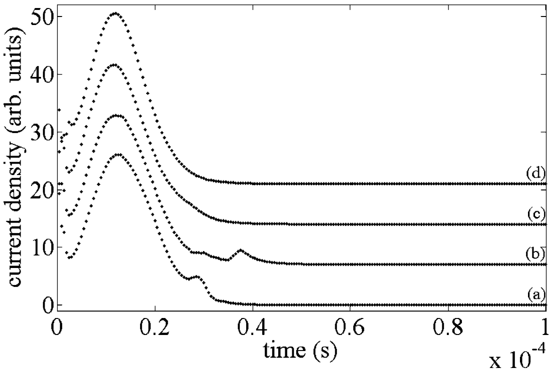

FIG. 10. As in Fig. 6 but with an amplitude for the electric pulse of 12 V/μm.

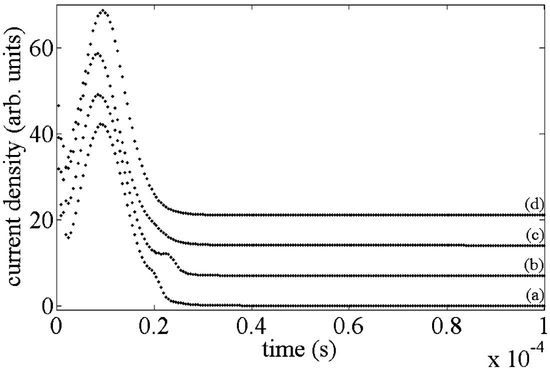

FIG. 12. As in Fig. 6 but with an amplitude for the electric pulse of 14 V/μm.

upper anchoring angles, see Figs. 8–10. From amplitudes of 13 V/μm onward, the order dynamics is definitively faster for bulk order reconstruction phenomena than for surface biaxial ones, see Figs. 4(b) and 5(c), with no need for a fast bulk transition. It follows that surface and bulk order reconstruction do not coexist, at least in the range of the investigated electric field amplitudes. On the other hand, properly combining electric field amplitudes with the upper anchoring angles, a confining and a squeezing of the order reconstruction into the surface biaxial wall can be obtained, similarly to what was observed in nanoconfined nematic liquid crystals, either mechanically [24], in which the confinement induces a two-dimensional stretching of a defect structure, or electrically [26], in which a defect core stretches along a confining surface, increasing the biaxiality of the surface layer.

The outcomes of our numerical simulations are properly framed within the phase diagram of Fig. 13, where, on the horizontal axis, the investigated electric pulse amplitudes E are shown, and, on the vertical axis, the anchoring angles θ_u imposed on the upper boundary plate of the cell are shown. Several computations have been performed to search for the phase boundaries in the (E, θ_u) plane delimiting domains where the nematic texture follows different switching mechanisms. For each point in the plane we classify the corresponding texture as bulk switching (BS), surface switching (SS), or no switching (NS): Triangles, circles, and squares mark the phase boundaries, respectively, among NS-BS, NS-SS, and SS-BS phase domains. This results in a partition of the (E, θ_u) plane in three regions, within each homogeneous textures concerning their switching regime are mapped. The three boundary curves converge toward a region where, due to the competition between the two switching mechanisms, it is not possible to unambiguously assign a switching regime to the nematic texture. In such a region the phase diagram has been sampled with steps $\Delta E = 0.05$ V/μm, $\Delta\theta_u = 0.05^\circ$, and, therefore, the extrapolated triple point coordinates are $(E)_T = 12.575$ V/μm $\pm$ 0.025 V/μm and $(\theta_u)_T = 2.025^\circ \pm 0.025^\circ$.

We remark that the points corresponding to the biaxiality maps shown in Figs. 4(b) and 5(d) are placed, respectively, on the SS-BS and NS-SS boundary lines. In fact, a closer inspection reveals that, in Fig. 4(b), in addition to the surface order reconstruction transition, inside the bulk biaxial cluster a dip starts to form, which is the signature of an incipient bulk order reconstruction. On the other hand, inside the biaxial wall of Fig. 5(d), a weak uniaxial line can be detected, which is, in

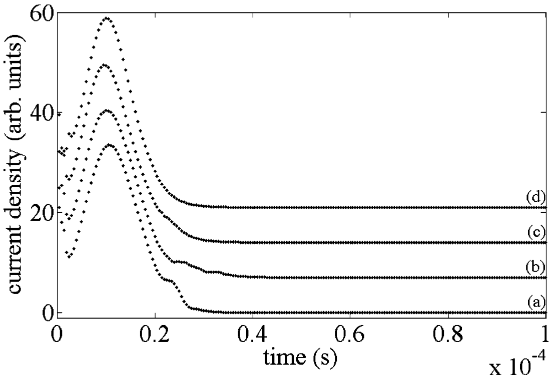

FIG. 11. As in Fig. 6 but with an amplitude for the electric pulse of 13 V/μm.

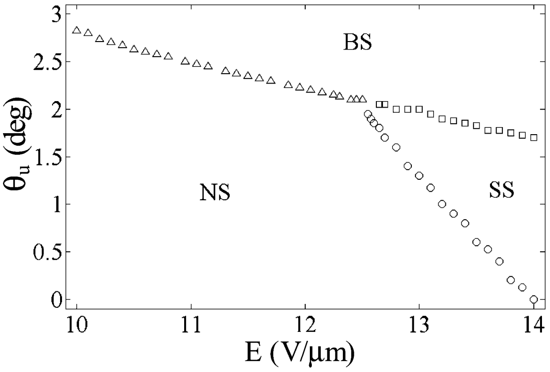

FIG. 13. Phase diagram in the plane (E, θ_u) for the occurrence of the bulk switching (BS), surface switching (SS), or no switching (NS) in the nematic texture. On the horizontal axis are reported the amplitudes of the applied electric pulse, while on the vertical axis are represented the anchoring angles imposed on the upper boundary plate of the π cell. For each simulation, the switching mechanism shown by the nematic texture has been referred to BS, SS, and NS. Triangles, circles, and squares represent the phase boundaries between the three switching regimes in the plane (E, θ_u). The triple point coordinates are $(E)_T = 12.575$ V/μm + 0.025 V/μm, and $(\theta_u)_T = 2.025^\circ + 0.025^\circ$.

turn, the signature of an incipient surface order reconstruction transition extending for several microseconds.

V. CONCLUSIONS

In this work we presented a moving mesh partial differential equations finite element method simulation applied to a dynamical **Q**-tensor model for the study of nematic liquid crystals confined in a π cell with asymmetric anchoring conditions. The parameters have been set in order to simulate different realistic asymmetric configurations of a π cell containing nematic material.

We computed the evolution of both the biaxiality and the current flowing across the cell after the application of electric fields with variable amplitudes. Selecting properly the amplitudes of the electric pulse and the geometric constraints at the boundary surfaces, either bulk or surface order reconstruction transition can occur. In fact, by applying a strong electric field and varying the pretilt upper angle, we can observe different mechanisms capable of relaxing the electrically induced nematic strain. In the first one, if the upper angle is not planar, the energy of the biaxial wall is released in a short time, building a well-defined electric peak corresponding to the well-known order reconstruction phenomenon, whereas, if the upper angle is approximately planar, the distortion energy is released more slowly during the motion of the biaxial wall toward the surface plate, with a wider electric signal. In addition, once the slow biaxial wall reaches the bounding plate and spreads over it, for strong-enough electric fields a surface order reconstruction transition occurs. Such behavior is not obvious and is reminiscent of surface defect spreading in hybrid homeotropic-planar cells in the presence of a strong electric field [26] or under nanoconfinement [24]. Moreover, at a given anchoring angle, the velocity of the biaxial features increases according to the amplitude of the applied electric pulse, while, at a given pulse amplitude, such velocity increases according to the decreasing anchoring angles. Nevertheless, at higher amplitudes of applied fields, two velocity rates are detected, respectively, below and above the bulk order reconstruction transition threshold. The above considerations suggest a possible way to drive, spatially and/or temporally, the biaxial phenomena arising inside the cell, a feature which could be important for application purposes.

The computed phase diagram allows us to map the nematic textures into regions characterized by their switching mechanism, against applied voltages on the cell plates and pretilt angles on the upper boundary surface.

The combined study of the temporal evolution of both the biaxiality and the current flow inside the π cell turns out to be a powerful method to investigate biaxial phenomena induced by fast electric distortion. The advantage is enhanced by the numerical method used to allow detailed computations of the **Q**-tensor dynamics inside the asymmetric cell: In fact, the grid points are driven inside the computational domain by $\nabla \mathbf{Q}$, which, in turn, grows according to the nematic distortion induced by the variable asymmetry. Our computational method allows an overall saving of computational effort with respect to the use of uniform grids, gaining new insights in the study of highly frustrated nematic molecules, a scenario mimicking realistic conditions. Work is in progress to numerically investigate the order dynamics in π cells under various geometrical and electrical conditions.

---

[1] N. J. Mottram and C. J. P. Newton, University of Strathclyde, Tech. Report No. 10, 2004.

[2] C. W. Oseen, Trans. Faraday Soc. **29**, 883 (1933); F. Franck, Discuss. Faraday Soc. **25**, 19 (1958).

[3] Y. Yi, G. Lombardo, N. Ashby, R. Barberi, J. E. Maclennan, and N. A. Clark, Phys. Rev. E **79**, 041701 (2009).

[4] E. Tjipto *et al.*, Nano Lett. **6**, 2243 (2006).

[5] F. Aliev and S. Basu, J. Non-Cryst. Solids **352**, 4983 (2006).

[6] M. Kleman and O. D. Lavrentovich, Philos. Mag. **86**, 4117 (2006).

[7] N. Schopohl and T. J. Sluckin, Phys. Rev. Lett. **59**, 2582 (1987).

[8] M. Buscaglia, G. Lombardo, L. Cavalli, R. Barberi, and T. Bellini, Soft Matter **6**, 5434 (2010).

[9] I. Musevic *et al.*, Science **313**, 954 (2006).

[10] I. I. Smalyukh, O. D. Lavrentovich, A. N. Kuzmin, A. V. Kachynski, and P. N. Prasad, Phys. Rev. Lett. **95**, 157801 (2005).

[11] J. C. Loudet, P. Hanusse, and P. Poulin, Science **306**, 1525 (2004).

[12] P. Biscari and P. Cesana, Continuum Mech. Therm. **19**, 285 (2007).

[13] P. G. de Gennes and J. Prost, *The Physics of Liquid Crystals* (Clarendon Press, Oxford, 1993); P. G. de Gennes, Phys. Lett. A **30**, 454 (1969).

[14] M. J. Freiser, Phys. Rev. Lett. **24**, 1041 (1970).

[15] T. Qian and P. Sheng, Liq. Cryst. **26**, 229 (1999).

[16] P. Martinot-Lagarde, H. Dreyfus-Lambez, and I. Dozov, Phys. Rev. E **67**, 051710 (2003).

[17] P. Biscari, G. Napoli, and S. Turzi, Phys. Rev. E **74**, 031708 (2006).

[18] M. Ambrožic, S. Kralj, and E. G. Virga, Phys Rev E **75**, 031708 (2007).

[19] R. Barberi, F. Ciuchi, G. Durand, M. Iovane, D. Sikharulidze, A. M. Sonnet, and E. G. Virga, Eur. Phys. J. E **13**, 61 (2004).

[20] R. Barberi, F. Ciuchi, G. Lombardo, R. Bartolino, and G. E. Durand, Phys. Rev. Lett. **93**, 137801 (2004); S. Joly, I. Dozov, and P. Martinot-Lagarde, *ibid.* **96**, 019801 (2006); R. Barberi, F. Ciuchi, H. Ayeb, G. Lombardo, R. Bartolino, and G. E. Durand, *ibid.* **96**, 019802 (2006).

[21] F. Ciuchi, H. Ayeb, G. Lombardo, R. Barberi, and G. E. Durand, Appl. Phys. Lett. **91**, 244104 (2007).

[22] G. Lombardo, H. Ayeb, F. Ciuchi, M. P. De Santo, R. Barberi, R. Bartolino, E. G. Virga, and G. E. Durand, Phys. Rev. E **77**, 020702 (2008).

[23] H. Ayeb, F. Ciuchi, G. Lombardo, and R. Barberi, Mol. Cryst. Liq. Cryst. **481**, 73 (2008).

[24] G. Carbone, G. Lombardo, R. Barberi, I. Musevic, and U. Tkalec, Phys. Rev. Lett. **103**, 167801 (2009).

[25] E. G. Virga, *Variational Theories for Liquid Crystal* (Chapman & Hall, London, 1994).
[26] G. Lombardo, H. Ayeb, and R. Barberi, Phys. Rev. E **77**, 051708 (2008).
[27] H. Ayeb, G. Lombardo, F. Ciuchi, R. Hamdi, A. Gharbi, G. E. Durand, and R. Barberi, Appl. Phys. Lett. **97**, 104104 (2010).
[28] G. Lombardo, A. Amoddeo, H. Ridha, H. Ayeb, and R. Barberi, Eur. Phys. J. E **35**, 9711 (2012).
[29] R. Barberi and G. E. Durand, Appl. Phys. Lett. **58**, 2907 (1991).
[30] C. H. Lee, E. P. Raynes, and S. J. Elston, Appl. Phys. Lett. **97**, 153501 (2010).
[31] T. Tang, Contemp. Math. **383**, 141 (2005).
[32] A. Amoddeo, R. Barberi, and G. Lombardo, Comput. Math. Appl. **60**, 2239 (2010).
[33] A. Amoddeo, R. Barberi, and G. Lombardo, Liq. Cryst. **38**, 93 (2011).
[34] A. M. Sonnet, P. Maffettone, and E. G. Virga, J. Non-Newtonian Fluid Mech. **119**, 51 (2004).
[35] A. M. Sonnet and E. G. Virga, Phys. Rev. E **64**, 031705 (2001).
[36] P. D. Brimicombe and E. P. Raynes, Liq. Cryst. **32**, 1273 (2005).
[37] J. Anderson, P. Watson, and P. Bos, in *LC3D: Liquid Crystal Display 3-D Directory Simulator, Software and Technology Guide* (Artech House, Boston, 1999).
[38] A. Alexe-Ionescu, Phys. Lett. A **180**, 456 (1993).
[39] G. Beckett, J. A. Mackenzie, A. Ramage, and D. M. Sloan, J. Comput. Phys. **167**, 372 (2001).
[40] C. de Boor, in *Conference on the Applications of Numerical Analysis, Dundee, 1973*, edited by J. Morris, Lecture Notes in Mathematics (Springer-Verlag, Berlin, 1974), Vol. 263, p. 12; V. Pereyra and E. G. Sewell, Numer. Math. **23**, 261 (1975); R. D. Russell and J. Christiansen, SIAM J. Numer. Anal. **15**, 59 (1978); A. B. White, *ibid.* **16**, 472 (1979).
[41] A. Ramage and C. J. P. Newton, Liq. Cryst. **34**, 479 (2007).
[42] G. Beckett and J. A. Mackenzie, Appl. Numer. Math. **35**, 87 (2000).
[43] W. Huang, J. Comput. Phys. **171**, 753 (2001).
[44] W. Huang, Y. Ren, and R. D. Russell, SIAM J. Numer. Anal. **31**, 709 (1994).
[45] P. Biscari, G. Peroli, and T. J. Sluckin, Mol. Cryst. Liq. Cryst. Sci. Technol., Sect. A **292**, 91 (1997).
[46] COMSOL MULTIPHYSICS [http://www.comsol.com/; MATLAB, http://www.mathworks.com].
[47] O. Zienkiewicz and R. Taylor, *The Finite Element Method* (Butterworth-Heinemann, Oxford, 2002), Vol. 1; Y. Known and H. Bang, *The Finite Element Method using Matlab* (CRC Press, Boca Raton, FL, 2000).
[48] B. Ratna and R. Shashidhar, Mol. Cryst. Liq. Cryst. **42**, 113 (1977).
[49] A. L. Alexe-Ionescu, R. Barberi, M. Giocondo, G. Cnossen, and T. H. van der Donk, Appl. Phys. Lett. **66**, 1701 (1995).
[50] M. Ambrožic, F. Bisi, and E. G. Virga, Continuum Mech. Thermodyn. **20**, 193 (2008).